Cell Reports

Article

miRNA-GABA influences female *Aedes aegypti* reproduction by modulating midgut homeostasis

Graphical abstract

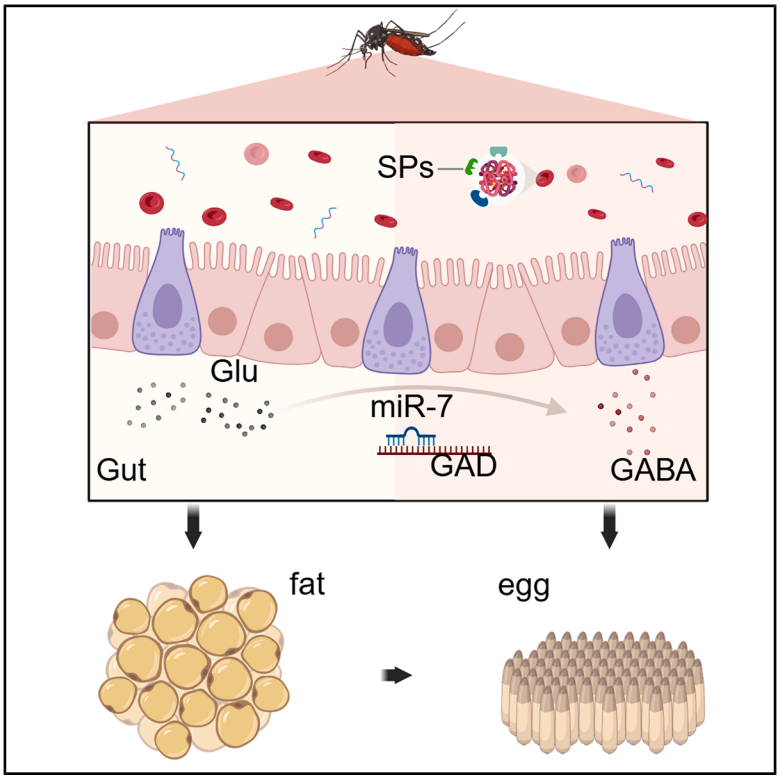

Authors

Jianping Cao, Lin Ling

Correspondence

linglin1000@163.com

In brief

Cao et al. identify miR-7 as a blood meal digestion regulator in *Aedes aegypti* females through sRNA-seq and physiological assays. CRISPR-Cas9-mediated miR-7 knockout combined with GABA delivery via the digestive tract reveals that midgut dysfunction subsequently impairs reproductive fitness.

Highlights

- miR-7 is strongly associated with blood meal digestion efficiency of *Ae. aegypti* females
- miR-7 directly targets GAD to modulate Glu-GABA homeostasis in the midgut
- Midgut dysfunction caused by digestive disorders impairs reproductive output in *Ae. aegypti*

Cao & Ling, 2025, Cell Reports *44*, 115776
June 24, 2025
https://doi.org/10.1016/j.celrep.2025.115776

CellPress

Cell Reports

CellPress
OPEN ACCESS

Article

miRNA-GABA influences female *Aedes aegypti* reproduction by modulating midgut homeostasis

Jianping Cao[1] and Lin Ling[1,2,*]
[1]School of Life Science and Technology, The Key Laboratory of Developmental Genes and Human Disease, Southeast University, Nanjing 210096, China
[2]Lead contact
*Correspondence: linglin1000@163.com
https://doi.org/10.1016/j.celrep.2025.115776

SUMMARY

Aedes aegypti's exceptional reproductive capacity drives the global proliferation of vector-borne diseases, including dengue, Zika, and chikungunya, while its hematophagous digestion supplies essential energy to catalyze critical reproductive processes. Our study reveals a significant microRNA (miRNA)-mediated mechanism. We demonstrate that miRNA-7 (miR-7) regulates γ-aminobutyric acid (GABA) levels in the midgut, thereby maintaining intestinal homeostasis. Comprehensive small RNA sequencing identifies miR-7 as a key regulatory molecule sensitive to blood meal digestion kinetics. Mechanistically, miR-7 directly targets glutamate decarboxylase to modulate the glutamate-GABA metabolic balance in the midgut. Concomitantly, female mosquitoes exhibit compromised midgut protease activity, disrupted fat body lipid storage, and diminished fecundity. This study delineates a hierarchical regulatory framework wherein miR-7-GABA modulates the efficiency of blood meal digestion and ultimately governs reproductive fitness.

INTRODUCTION

The persistent transmission of arboviruses by *Aedes aegypti* imposes a profound global health burden, with this mosquito species alone responsible for over 400 million dengue infections annually.[1,2] This epidemiological significance stems from its blood-feeding behavior and exceptional reproductive plasticity.[3,4] Female mosquitoes undergo multiple (>3) reproductive cycles in their lifetime, each yielding approximately 120 eggs through tightly coordinated blood meal utilization and ovarian maturation.[4,5] A defining feature of *Ae. aegypti*'s reproductive biology is its biphasic life history, alternating between post-eclosion (PE) and post-blood-meal (PBM) stages.[6,7] During the 72-h PE phase, newly emerged adults sustain survival on nectar-derived carbohydrates while developing host-seeking behaviors.[8,9] The PBM phase, initiated by blood feeding, triggers a metabolic cascade: midgut proteases degrade hemoglobin (HGB) into amino acids that fuel yolk synthesis.[10–12] Concurrently, blood meal digestion over 72 h remodels fat body composition via hormonal and nutrient signaling pathways, mobilizing lipid reserves to support ovarian development.[13–15] The critical role of digestive physiology in reproductive output underscores the necessity of dissecting its regulatory architecture.

MicroRNAs (miRNAs) are evolutionarily conserved non-coding RNAs that exert precise spatiotemporal control over target gene expression through 5′ seed region (nucleotides [nt] 2–8)-mediated mRNA degradation.[16–19] While prior studies have explored miRNA-regulated blood meal digestion in *Ae. aegypti* through various mechanisms,[20–23] few have systematically investigated the miRNAs that modulate HGB digestion kinetics. In this study, we identified miRNA-7 (miR-7) as a key regulator of HGB digestion rate using high-throughput small RNA sequencing (sRNA-seq) combined with digestion rate assays. CRISPR-Cas9 mutagenesis combined with target validation revealed that miR-7 deletion disrupted midgut glutamate (Glu)- γ-aminobutyric acid (GABA) homeostasis by derepressing glutamate decarboxylase (GAD). This neuroendocrine imbalance directly manifested as delayed blood meal processing, secondary to impaired lipid storage, and arrested ovarian development, ultimately reducing reproductive fitness. Our study established an important miRNA that influences reproductive output through the modulation of digestion, offering significant targets for interventions aimed at disrupting arbovirus transmission.

RESULTS

Dynamic regulation of midgut miR-7 expression correlates with HGB digestion kinetics in *Ae. aegypti*

To assess blood digestion dynamics, we quantified HGB levels in the midgut at sequential PBM time points. While HGB content progressively decreased, digestion kinetics exhibited a biphasic pattern, peaking approximately 24 h after the blood meal (24 h PBM) (Figures 1A and S1A). To investigate transcriptional regulation during this process, we performed sRNA-seq on midgut tissues 24 h PBM and 72 h PE. Multidimensional analyses (principal-component analysis [PCA] and sample clustering) revealed significant transcriptional divergence between the two groups, with intragroup reproducibility maintained across technical replicates (Figures S2A and S2B). The dataset comprised 188 miRNAs, with differential expression analysis identifying 30 upregulated and

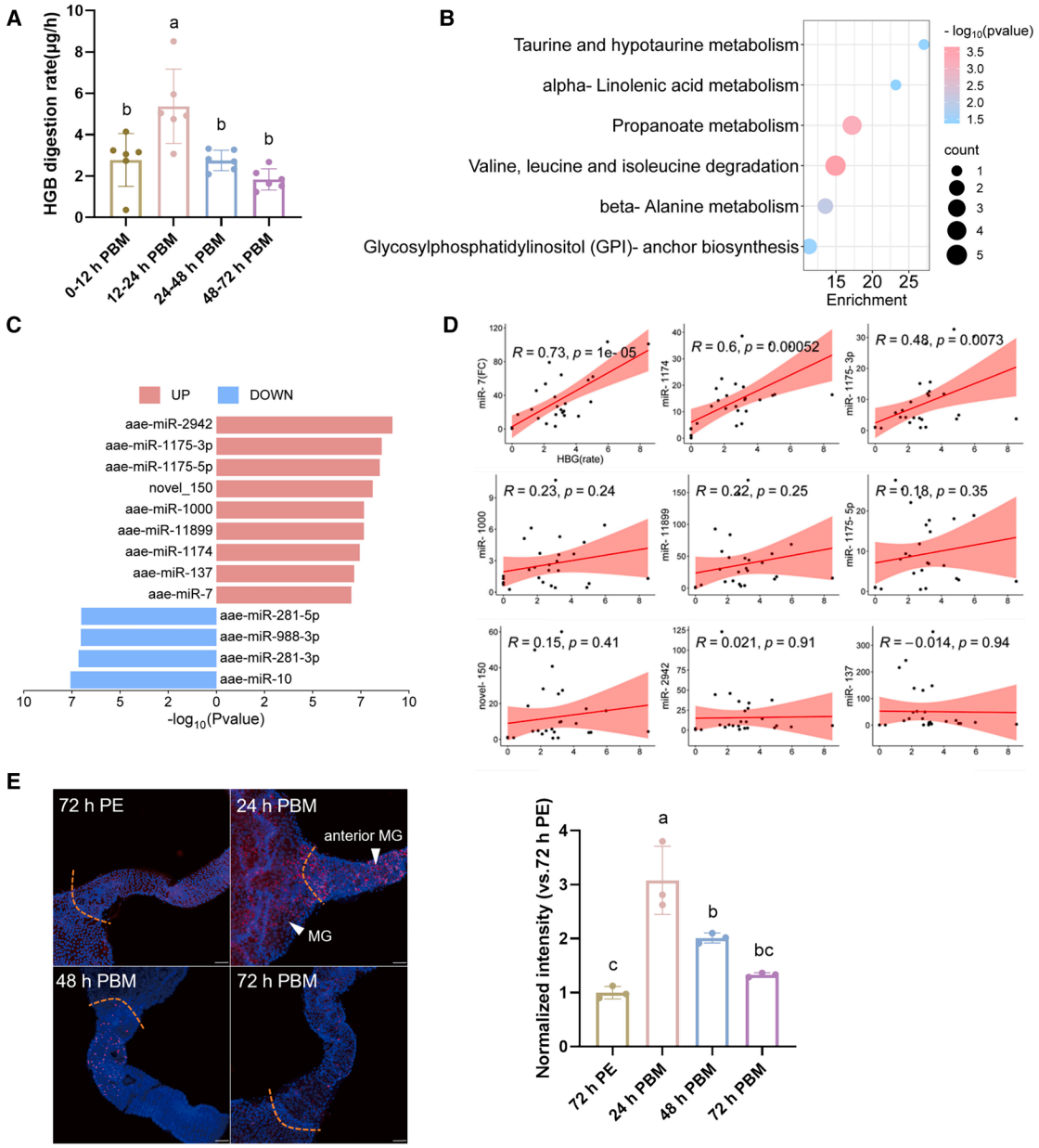

Figure 1. Changes in miR-7 expression in the midgut in response to a blood meal

(A) Quantification of hemoglobin (HGB) digestion efficiency in the midgut across distinct temporal intervals following a blood meal.

(B) Kyoto Encyclopedia of Genes and Genomes (KEGG) pathway analysis revealed that target genes of differentially expressed miRNAs 24 h post-blood meal (PBM) are predominantly enriched in amino acid metabolism-related pathways.

(C) sRNA-seq identified the miRNAs exhibiting the most significant differential expression ($|\log_{10}(p \text{ value})| > 7$) in the midgut 24 h PBM.

(D) Correlation analysis demonstrates the relationship between miRNA fold change (qPCR quantification, *y* axis) and HGB digestion rate (ELISA measurement, *x* axis) across each temporal interval after blood feeding. FC, fold change.

(E) RNA fluorescence *in situ* hybridization (FISH) reveals significant upregulation of miR-7 expression in the midgut 24 h PBM, with predominant localization at the anterior midgut during other temporal intervals (scale bar: 50 μm). MG, midgut.

Data are represented as means ± SEM. ns $p > 0.05$, $^{*}p < 0.05$, $^{**}p < 0.01$, and $^{***}p < 0.001$.

42 downregulated miRNA candidates (Figures S2C and S2D). To validate the transcriptomic findings, we conducted quantitative polymerase chain reaction (qPCR)-based verification of selected miRNAs at the corresponding time points (Figure S2E). Kyoto Encyclopedia of Genes and Genomes (KEGG) pathway enrichment analysis revealed that differentially expressed miRNAs 24 h PBM were predominantly associated with amino acid metabolism pathways in the midgut (Figure 1B).

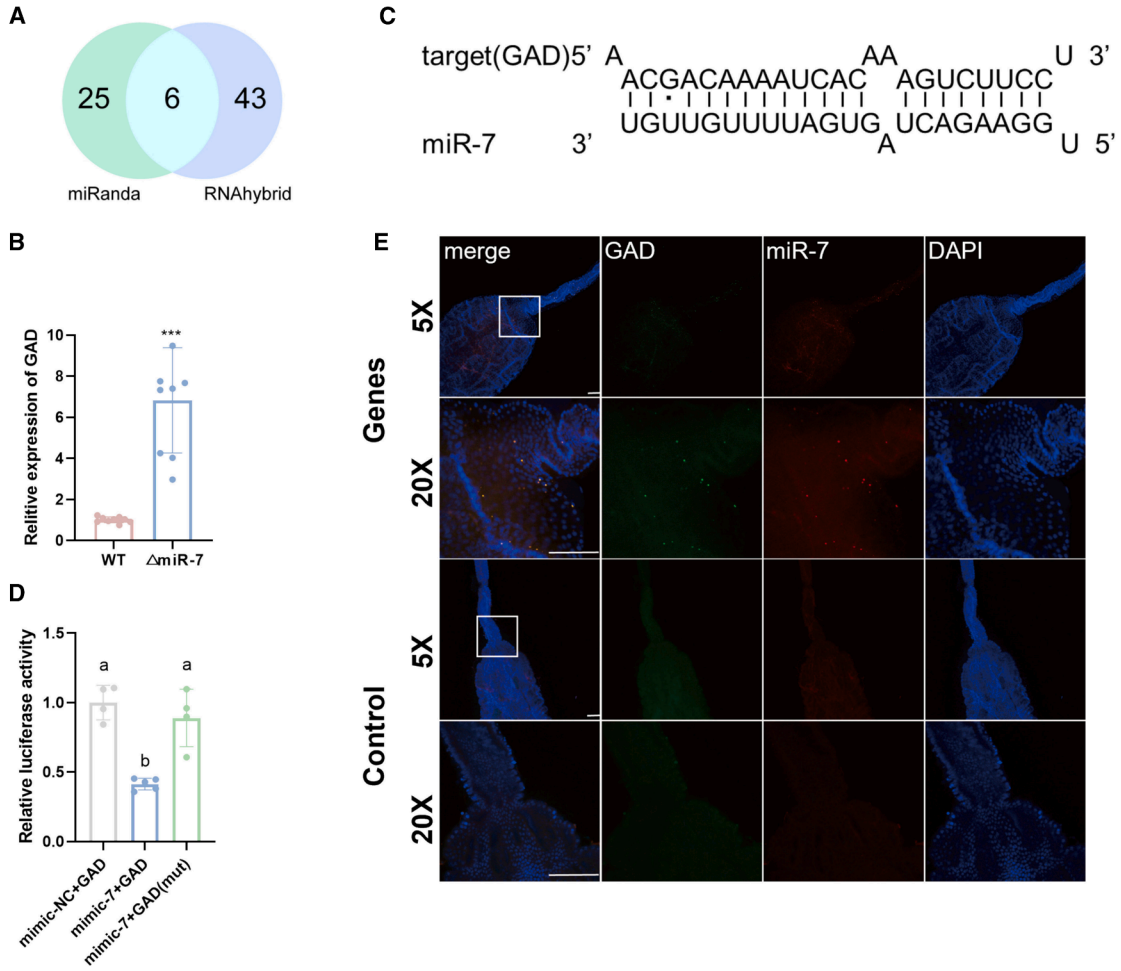

Figure 2. Identification of glutamate decarboxylase as a miR-7 target in *Aedes aegypti*

(A) The intersection of miRanda and RNAhybrid predictions identifies six potential targets.

(B) Significantly enriched glutamate decarboxylase (GAD) transcripts were observed following miR-7 disruption.

(C) Computational prediction algorithms identified the putative miR-7 binding sites in GAD.

(D) The dual luciferase reporter gene assay demonstrates miR-7-targeted binding to GAD *in vitro*.

(E) Double FISH reveals co-localization of miR-7 and GAD *in vivo* 24 h PBM (scale bar: 100 μm).

Data are represented as means ± SEM.

We prioritized miRNAs exhibiting high statistical significance ($-\log_{10}(p$ value) > 7; Figure 1C) for functional analysis. Among the upregulated miRNAs, a systematic correlation of expression profiles with HGB digestion kinetics across multiple time points identified miR-7 as a key regulatory candidate whose temporal expression pattern exhibited strong alignment with HGB digestion dynamics (Figures 1D and S1B). qPCR analysis confirmed elevated miR-7 expression during early PBM stages (24 h) compared with that at 72 h PE, with the highest abundance detected in the midgut, fat body, and Malpighian tubules (Figure S3). Spatial localization studies via fluorescence *in situ* hybridization (FISH) revealed dynamic miR-7 distribution. At 72 h PE, low-level signals were restricted to the anterior midgut. Following blood ingestion, miR-7 expression expanded throughout the midgut 24 h PBM before retracting to the junctional region by 48 h PBM (Figure 1E). These spatiotemporal patterns suggest that miR-7 plays a role in modulating blood digestion processes.

miR-7 directly targets GAD in Glu-GABA homeostasis

To identify potential miR-7 target genes in *Ae. aegypti*, computational predictions were performed using two complementary algorithms: miRanda (http://www.microrna.org/microrna/home.do) and RNAhybrid (https://bibiserv.cebitec.uni-bielefeld.de/rnahybrid). The miRanda algorithm identified 31 candidate targets (Table S1), and RNAhybrid predicted 49 putative targets (Table S2). The intersection of these two datasets revealed six common target genes (Figure 2A). Among these, GAD emerged as a notable candidate because of its critical role in insect amino acid metabolism and involvement in GABA biosynthesis.[24,25]

We generated miR-7-deficient mosquitoes (*ΔmiR-7*) using CRISPR-Cas9 technology. Following a standard protocol,

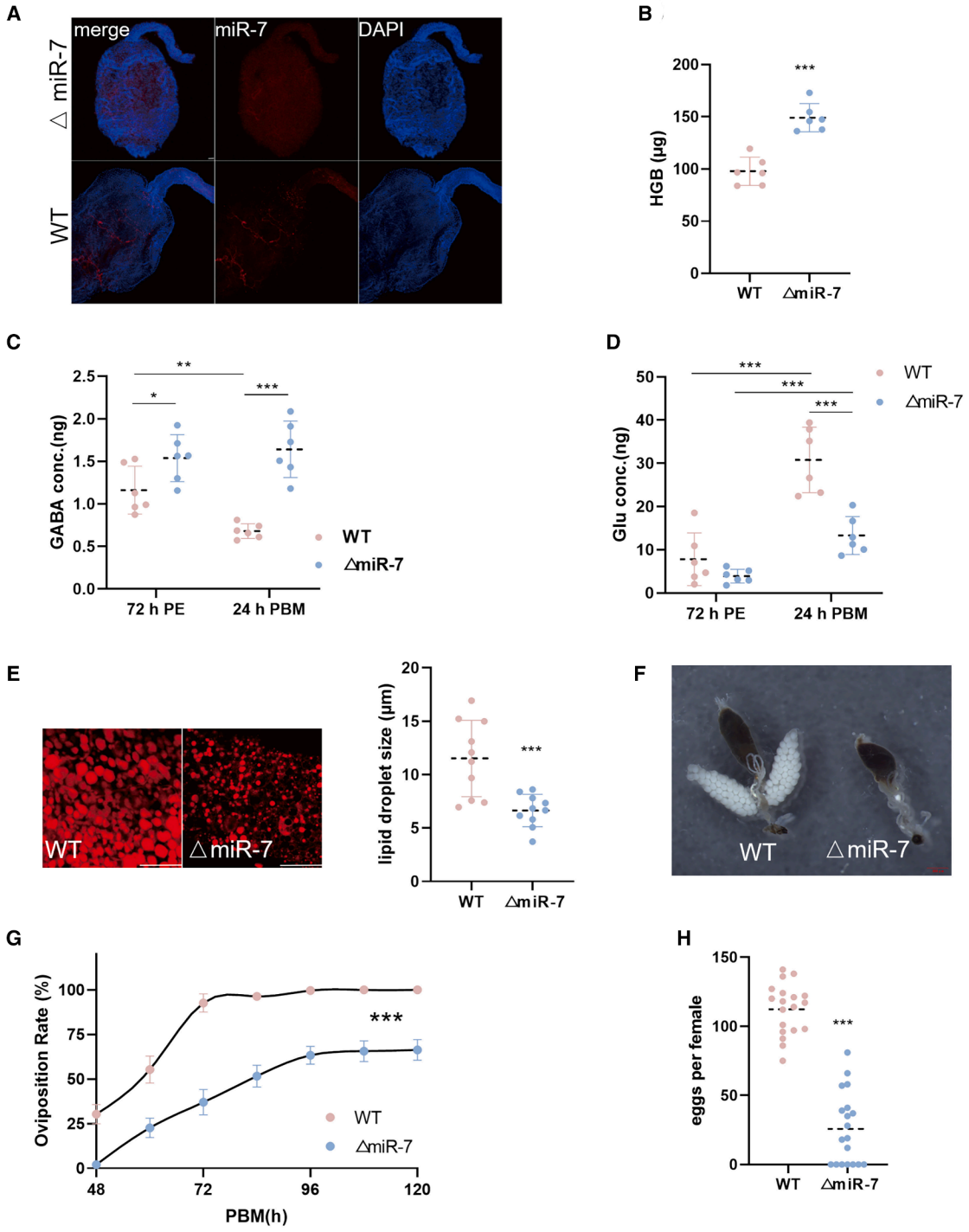

Figure 3. Disruption of the miR-7 genome by CRISPR-Cas9 affects the physiological state of *Aedes aegypti*

(A) RNA FISH demonstrates complete absence of miR-7 expression in the midgut 24 h PBM and post-knockout (scale bar: 50 μm).

(B) ELISA quantification revealed significantly altered HGB content in blood clots of midguts from wild-type (WT) and *ΔmiR-7* females 24 h PBM.

(C and D) Quantitative ELISA analysis shows differential γ-aminobutyric acid (GABA) and glutamate (Glu) levels in midguts of WT vs. *ΔmiR-7* females 72 h post-eclosion (PE) and 24 h PBM.

(E) Nile red staining of fat body lipid droplets in WT and *ΔmiR-7* females (with undeveloped ovaries) 24 h PBM, visualized by confocal microscopy (scale bar: 50 μm).

(F) Histological imaging of dissected intestines and ovaries from WT and *ΔmiR-7* females 24 h PBM (scale bar: 300 μm).

(legend continued on next page)

embryos were injected with a mixture of single-guide RNA (sgRNA) (40 ng/μL) and recombinant Cas9 protein (333 ng/μL) at 2 h post-oviposition. qPCR analysis of adult female mosquitoes demonstrated that GAD transcript levels were significantly upregulated in *ΔmiR-7* individuals compared with those in wild-type (WT) controls 24 h PBM (Figure 2B). Spatial analysis revealed that GAD and miR-7 exhibited similar localization patterns but maintained a negative expression correlation in midgut tissues across multiple time points (Figures 1E and S4), suggesting a potential functional interaction.

Computational predictions identified a conserved miR-7 binding site within the GAD 3′ untranslated region (UTR) (Figure 2C). To validate this interaction, we constructed two reporter plasmids containing WT (*GAD*) and mutant *GAD* (*mut*) GAD 3′ UTR fragments, which were inserted into the NotI site of the psi-CHECK2 vector (Figure S5). Luciferase activity assays in *Drosophila* Schneider 2 (S2) cells showed that co-transfection with the miR-7 mimic significantly reduced reporter expression compared with the negative control (mimic-NC) (Figure 2D). Mutagenesis of the miR-7 seed sequence in the GAD reporter restored the luciferase activity to baseline levels (Figure 2D), confirming sequence-specific target recognition. To further establish this interaction *in vivo*, we performed FISH. The results demonstrated the co-localization of miR-7 and GAD transcripts in midgut tissues (Figure 2E), providing direct evidence for their spatial association and functional pairing.

CRISPR-Cas9-mediated miR-7 deficiency disrupts midgut homeostasis and induces reproductive dysfunction in blood-fed females

To investigate the functional consequences of miR-7 deficiency in female *Ae. aegypti*, we analyzed the CRISPR-Cas9-generated *ΔmiR-7* mutants. Approximately 31% of injected embryos survived to adulthood, with a female-to-male ratio of 85:82, and underwent systematic phenotypic characterization. Sanger sequencing revealed extensive sequence variations in the mature miR-7 region and its flanking sequences (Figure S6A), confirming successful locus disruption via CRISPR-Cas9. qPCR and FISH analyses demonstrated a significant reduction in miR-7 expression levels in the midguts of *ΔmiR-7* females compared with those in WT controls (Figures 3A and S6B).

At 24 h PBM, we assessed blood digestion efficiency and Glu-GABA homeostasis in *ΔmiR-7* females. Loss of miR-7 function caused pronounced digestive dysfunction, evidenced by an ∼0.5-fold increase in midgut HGB content in *ΔmiR-7* females relative to that of the WT controls (Figure 3B). GABA biosynthesis analysis revealed dysregulated temporal expression patterns: while WT females exhibited a 0.5-fold decrease in midgut GABA content from 72 h PE to 24 h PBM, *ΔmiR-7* females maintained elevated GABA levels across both time points (Figure 3C). This was accompanied by altered Glu dynamics: although both genotypes showed increased Glu accumulation post-blood feeding, *ΔmiR-7* females exhibited 50% lower Glu levels 24 h PBM compared with those of the WT (Figure 3D). In summary, miR-7 deficiency disrupts Glu-GABA metabolic homeostasis in the midgut and is accompanied by midgut digestive dysfunction.

Given the critical functional interplay between fat body lipid metabolism and midgut blood meal digestion,[26,27] we assessed lipid storage using Nile red staining. At 24 h PBM, *ΔmiR-7* females exhibited significantly smaller lipid droplets in the fat body compared with those in WT controls (Figure 3E). Since normal digestive processes and lipid metabolic pathways are essential for ovarian development,[27–29] we performed histological analysis of *ΔmiR-7* female ovaries, which revealed that *ΔmiR-7* female individuals identified as mutants had severe developmental abnormalities: their bilateral ovaries either completely lacked developing follicles or displayed unilateral follicular development (Figures 3F and S6C–S6E). Collectively, these observations imply that miR-7 deficiency disrupts lipid biosynthetic pathways by influencing blood meal digestion, ultimately leading to ovarian dysmorphogenesis.

To evaluate reproductive behavior, we quantified oviposition rates using a standardized protocol. Fifty females per group were monitored across six experimental replicates. Oviposition assays were conducted every 12 h, starting at 48 h PBM, with each female placed on a moist filter paper for 3 h under controlled environmental conditions. *ΔmiR-7* females exhibited significantly reduced oviposition rates (60% vs. 100% in the WT) and delayed oviposition kinetics, reaching peak egg deposition at 96 h PBM compared with that of the WT at 72 h PBM (Figure 3G). Although *ΔmiR-7* females produced ∼70% fewer eggs overall (Figure 3H), embryo hatchability rates remained comparable between genotypes (Figure S6F). Collectively, these findings demonstrate that miR-7 plays a pivotal role in maintaining reproductive fitness in female mosquitoes by regulating nutrient metabolism, which in turn affects ovarian development and oviposition behavior.

GAD interference restores the miR-7-deficient female phenotype

To determine whether GAD functions as a causal mediator between miR-7 deficiency and physiological dysfunction, we performed RNA interference rescue experiments using *ΔmiR-7* adult female mosquitoes 60 h PE. Experimental mosquitoes were treated with either *dsGAD* (*ΔmiR-7+iGAD*; targeting GAD) or *dsLuciferase* (*ΔmiR-7+iLuc*; NC) (Figure 4A). qPCR analysis revealed that GAD expression was specifically silenced in *ΔmiR-7+iGAD* compared with that in *ΔmiR-7+iLuc* across all time points (Figure 4B). Consistent with WT controls, *ΔmiR-7+iGAD* exhibited a biphasic GAD expression pattern—downregulated 24 h PBM and upregulated thereafter—confirming transcriptional rescue (Figure 4B). Spatial analysis further demonstrated that GAD expression localized to the anterior midgut in all groups 24 h PBM, mirroring miR-7 expression patterns (Figures 4C and 1E).

(G) Oviposition rate (every 50 females) analysis reveals significant differences between WT ($n = 6$) and *ΔmiR-7* ($n = 6$) females at multiple time points after blood feeding (***$p < 0.001$, final oviposition rate shown with statistical significance).
(H) Comparative egg count analysis demonstrates reduced fecundity in *ΔmiR-7* mutants compared to WT females ($n = 19$).
Data are represented as means ± SEM. ns $p > 0.05$, *$p < 0.05$, **$p < 0.01$, and ***$p < 0.001$.

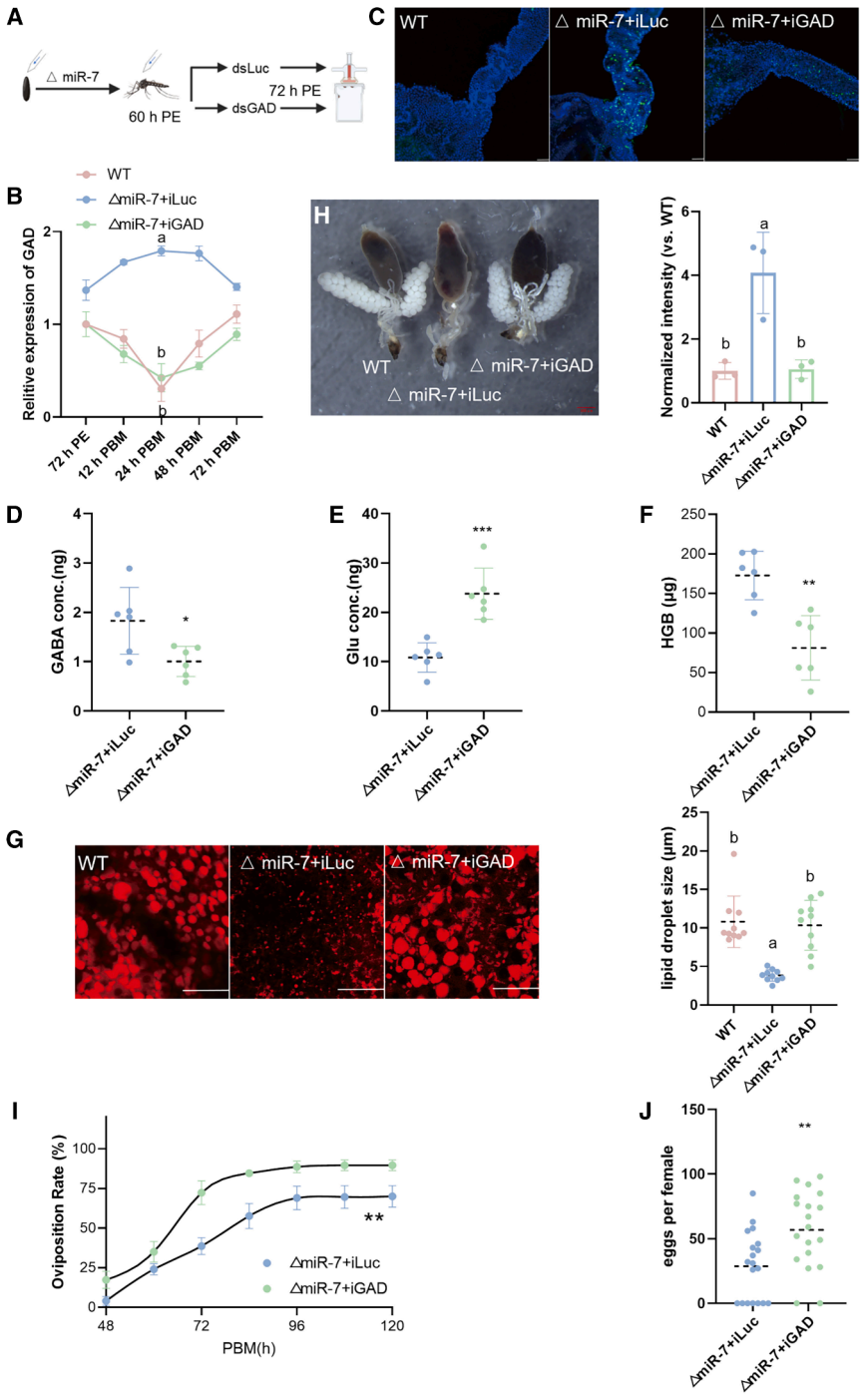

Figure 4. Interference with GAD can compensate for the losses caused by miR-7 deficiency

(A) Experimental design outline for functional rescue analysis.

(B) qPCR analysis reveals GAD mRNA expression levels in midguts of WT, *ΔmiR-7+iLuc*, and *ΔmiR-7+iGAD* females at pre- and post-blood-meal time points.

(C) RNA FISH visualization demonstrates GAD localization in midguts of WT, *ΔmiR-7+iLuc*, and *ΔmiR-7+iGAD* females 24 h PBM (scale bar: 50 μm; blue fluorescence: DAPI; green fluorescence: GAD).

(D–F) Quantitative ELISA analysis quantifies GABA, Glu, and HGB contents in intestines of *ΔmiR-7+iLuc* and *ΔmiR-7+iGAD* females 24 h PBM.

(G) Confocal microscopy imaging reveals lipid droplet accumulation in fat bodies of WT, *ΔmiR-7+iLuc* (with undeveloped ovaries), and *ΔmiR-7+iGAD* females 24 h PBM (scale bar: 50 μm).

(H) Histological analysis of dissected intestines and ovaries from WT, *ΔmiR-7+iLuc*, and *ΔmiR-7+iGAD* females 24 h PBM (scale bar: 500 μm).

(I) Oviposition rate (every 50 females) analysis compares fecundity between *ΔmiR-7+iLuc* and *ΔmiR-7+iGAD* groups (n = 6) at multiple post-blood-feeding time points (**$p < 0.01$, significant differences observed in final oviposition rates).

(J) Comparative egg count analysis demonstrates reduced fecundity in *ΔmiR-7+iGAD* mutants compared to *ΔmiR-7+iLuc* controls (n = 19).

Data are represented as means ± SEM. ns $p > 0.05$, *$p < 0.05$, **$p < 0.01$, and ***$p < 0.001$.

At 24 h PBM, *ΔmiR-7+iGAD* achieved ~60% GAD knockdown efficiency, accompanied by restored metabolic homeostasis: midgut GABA levels decreased by 40%, while Glu levels increased by 100% compared with those in *ΔmiR-7+iLuc* (Figures 4D and 4E). These metabolic improvements correlated with enhanced HGB digestion capacity (Figure 4F), leading to restored lipid metabolism in the fat body (Figure 4G) and the recovery of ovarian follicle development (Figures 4H and S7A).

Collectively, these data establish that GAD serves as a critical molecular hub through which miR-7 maintains midgut homeostasis, nutrient processing, and reproductive output in female *Ae. aegypti*.

Complementary fecundity analysis revealed that, compared with *ΔmiR-7+iLuc*, *ΔmiR-7+iGAD* females exhibited earlier oviposition and an increased oviposition rate (85% vs. 60% 84 h PBM) (Figure 4I). Moreover, *ΔmiR-7+iGAD* ovaries produced twice as many embryos as *ΔmiR-7+iLuc* ovaries, with comparable hatching rates (Figures 4J and S7B). Collectively, these findings demonstrate that GAD is an essential regulatory node that mediates the control of miR-7 over midgut physiology, nutrient utilization, and reproductive success in *Ae. aegypti* females.

GABA functions as a signaling transducer in the miR-7-GAD axis to mediate female physiological regulation

We have established that the female midgut miR-7-GAD axis regulates GABA synthesis. To investigate how GABA transmits

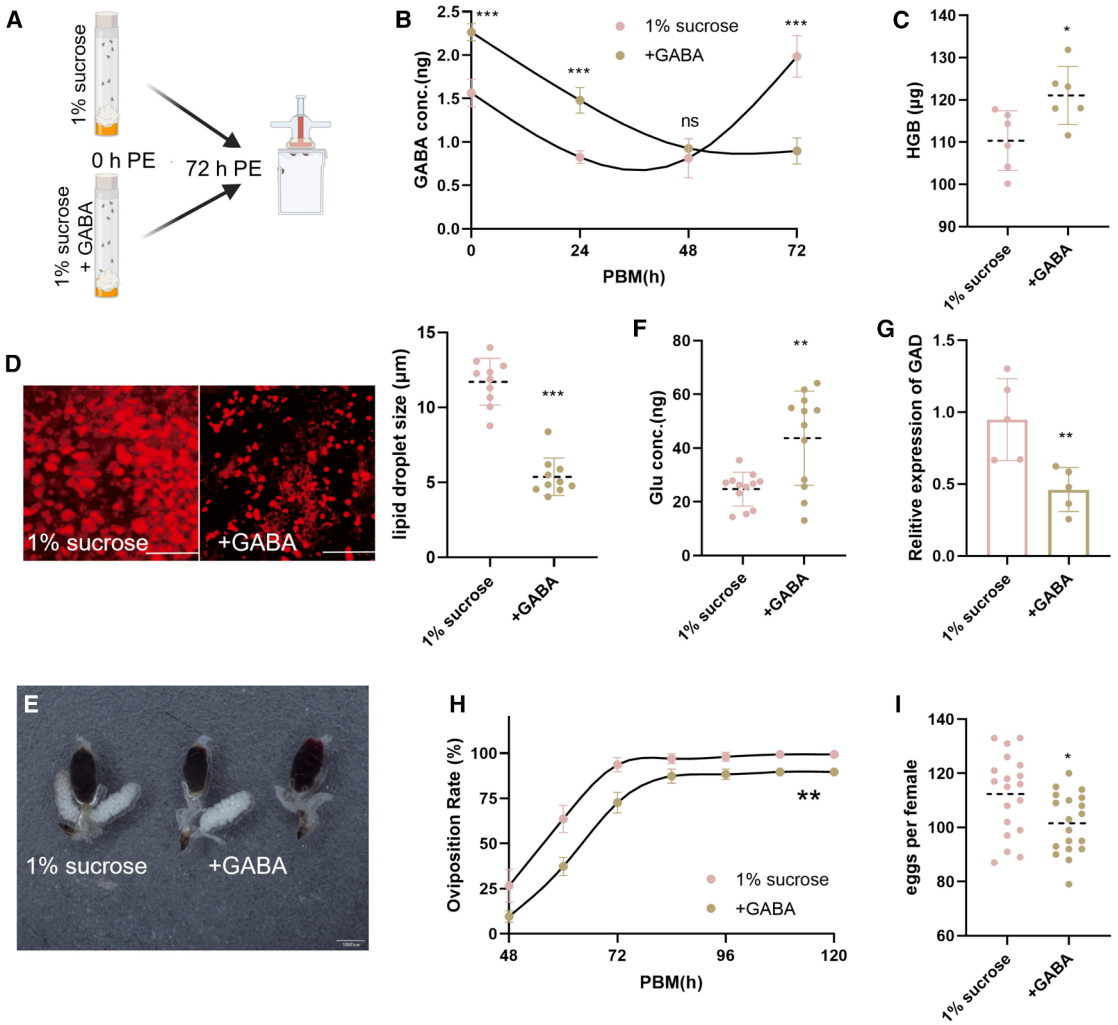

Figure 5. Excessive GABA on female *Aedes aegypti* mimics the effects of miR-7 deficiency

(A) Experimental mode.

(B) Quantitative ELISA analysis reveals GABA content variation in midguts of sucrose-fed and GABA-fed females across PBM time points.

(C and F) ELISA quantification shows differential HGB and Glu levels in midguts of sucrose-fed vs. GABA-fed females 24 h PBM.

(D) Confocal microscopy imaging visualizes lipid droplet accumulation in fat bodies of sucrose-fed and GABA-fed females (with undeveloped ovaries) 24 h PBM (scale bar: 50 μm).

(E) Histological analysis of dissected intestines and ovaries from sucrose-fed and GABA-fed females 24 h PBM (scale bar: 1,000 μm).

(G) qPCR quantification measures GAD mRNA expression levels in midguts of sucrose-fed and GABA-fed females 24 h PBM.

(H) Oviposition rate (every 50 females) analysis compares fecundity patterns between sucrose-fed and GABA-fed groups ($n = 6$) at multiple post-blood-feeding intervals (**$p < 0.01$, significant differences observed in final oviposition rates).

(I) Comparative egg count analysis demonstrates reduced fecundity in GABA-fed females compared with that in sucrose-fed controls ($n = 19$).

Data are represented as means ± SEM. ns $p > 0.05$, *$p < 0.05$, **$p < 0.01$, and ***$p < 0.001$.

miR-7-GAD regulatory functions and maintains physiological homeostasis in adult females, we performed feeding experiments using a GABA (1 mg/mL)-sucrose (1%) solution starting at adult emergence, with 1% sucrose solution serving as the control (Figure 5A). In sugar-fed females, GABA concentration exhibited a positive correlation with the WT midgut GAD expression pattern, showing a transient decrease followed by an increase during the PBM phase (Figures 5B and 4B). Notably, although GABA levels continued to decline after a blood meal in GABA-fed females, their midgut GABA levels were still significantly higher than those of females fed with 1% sucrose 24 h PBM (Figure 5B).

At 24 h PBM, GABA-fed females exhibited compromised blood digestion kinetics, reduced lipid droplet accumulation in fat bodies, and delayed ovarian development compared with sugar-fed controls (Figures 5C–5E). These phenotypic abnormalities closely resembled those observed in *ΔmiR-7* mutants, suggesting functional equivalence between miR-7 deficiency and GABA hyperactivation. Interestingly, unlike *ΔmiR-7* females, GABA-fed individuals exhibited reduced midgut Glu consumption

compared with controls (Figure 5F). qPCR analysis revealed an approximately 50% reduction in midgut GAD expression upon GABA treatment (Figure 5G), indicating a negative feedback mechanism in which exogenous GABA suppressed GAD expression and Glu metabolism.

GABA feeding caused persistent reproductive defects throughout the experimental period. Although the peak oviposition timing was not significantly altered, GABA-fed females exhibited substantially reduced final egg production (80% vs. 98% in controls) (Figure 5H). Additionally, compared with sucrose-fed controls, the number of embryos produced by GABA-fed female mosquitoes was approximately 80% of that of the control group, though embryo hatching rates remained comparable (Figures 5I and S8). Collectively, these findings establish that the miR-7-GAD-GABA axis is a critical regulatory network that controls midgut homeostasis in female *Ae*. *aegypti*, which has significant implications for reproductive output modulation.

The miR-7-GABA regulatory axis orchestrates serine protease homeostasis through modulating midgut cell apoptosis

Mammalian studies demonstrate that elevated GABA concentrations induce apoptosis through multiple molecular mechanisms.[30,31] To characterize how experimental manipulations affect blood meal digestion, we analyzed GABA receptor expression in the midgut and quantified midgut cell apoptosis following blood ingestion. At 24 h PBM, we identified a single GABA receptor homolog, the dieldrin resistance protein (RDL), in the midgut (Figure 6A). TUNEL staining was performed to quantify apoptotic indices in midgut tissues at 24 h PBM across experimental groups. *ΔmiR-7* females exhibited elevated apoptotic indices in midgut cells compared to WT controls, which were significantly reduced following GAD knockdown (Figure 6B). Midgut cell apoptosis was significantly elevated in GABA-fed females relative to sucrose controls (Figure 6B). Core apoptotic regulators Dronc and Ark showed significant positive correlations with midgut GABA levels, whereas anti-apoptotic IAP1/2/5/6 transcripts displayed inverse correlations (Figure 6C).[32] These findings collectively demonstrate that the miR-7-GABA axis orchestrates midgut cell apoptosis.

PBM digestive enzyme secretion is tightly regulated by the dynamic proliferation and differentiation of midgut cells.[33] Serine proteases (SPs) represent the primary enzymes that mediate blood digestion in the midgut of *Ae*. *aegypti*, with their abundance serving as a critical indicator of midgut digestive capacity.[10–12,34] To assess how apoptotic states influence protease secretion, we profiled major serine protease expression under experimental conditions. Both *ΔmiR-7* mutants and GABA-fed females exhibited SP expression levels comparable to those of WT controls at 72 h PE (Figure 6D). However, distinct temporal regulation patterns emerged: at 12 and 24 h PBM, most SPs (JA15, ET, SPI, LT, SPVI, and SPVII) were significantly downregulated in both *ΔmiR-7* and GABA-fed groups (Figure 6D). Notably, selected enzymes (LT, SPVI, and SPVII) maintained suppressed expression through 48 and 72 h PBM (Figure 6D). These collective findings demonstrate that GABA disrupts digestive enzyme secretion via induction of midgut cell apoptosis, with SP reduction emerging as a hallmark feature, particularly during the critical early phase ($\leq$24 h PBM).

DISCUSSION

Numerous studies have demonstrated that the midgut-fat body-ovary axis in female *Ae*. *aegypti* collaboratively maintains reproductive homeostasis.[15,35–38] This investigation identified a significant regulatory mechanism involving miR-7-GABA that mediates relevant physiological responses in this axis system by modulating blood meal digestion. HGB constitutes over 95% of the vertebrate blood protein content and serves as the primary nutritional substrate for reproductive energy production in *Ae*. *aegypti*.[39–41] Given this functional significance, we quantified digestion capacity through midgut consumption analysis after blood feeding. Our data revealed rapid HGB degradation 24 h PBM, consistent with prior investigations.[42–46] Transcriptomic analysis comparing 24 h PBM vs. 72 h PE revealed that differentially expressed miRNAs in the midgut primarily target amino acid metabolism pathways, aligning with their role in blood digestion processes.[43,46,47] The miRNA miR-7, identified through differential expression screening, exhibited inverse temporal expression patterns with its target gene GAD in the midgut while maintaining spatial co-localization. Such spatiotemporal regulation of miRNA targets has been documented in other systems,[48–52] corroborating the functional relationship between miR-7 and GAD. CRISPR-Cas9-mediated loss-of-function studies demonstrated that miR-7 deficiency induced midgut Glu-GABA metabolic imbalance through GAD overexpression, leading to digestive dysfunction. Rescue experiments confirmed that target gene manipulation can reverse miRNA-deficient phenotypes, which is a well-established method for validating miRNA regulatory specificity.[53,54] Specifically, GAD overexpression under miR-7-deficient conditions resulted in the elevation of GABA synthesis and subsequent digestive disorders. Conversely, GAD knockdown restored midgut GABA homeostasis and alleviated both metabolic and phenotypic abnormalities. Notably, this phenotypic rescue exhibited partial efficacy. We infer that this residual dysfunction may derive from the pleiotropic regulatory targets of miR-7, as supported by accumulating evidence from *Ae. aegypti* studies demonstrating functional redundancy among multi-target miRNAs.[55] Oral administration of exogenous GABA validated the tissue specificity of this regulatory network, as direct midgut delivery induced pathophysiological changes that mirrored miR-7 deficiency. Collectively, these findings established that miR-7 modulates digestive processes through GABA signaling via GAD regulation.

GABA, a non-proteinogenic amino acid with established roles in neurotransmission and metabolic regulation, has pleiotropic functions across diverse biological contexts.[56–58] In mammalian systems, GABA inhibits intestinal motility and modulates nutrient absorption efficiency.[59,60] Previous studies on high-fat-diet-induced obesity models have revealed GABA's inhibitory effects on adipogenesis.[61] Our data suggest that elevated midgut GABA levels may similarly disrupt digestive homeostasis in mosquitoes, potentially through mechanisms involving midgut cell apoptosis and secretory function modulation. The observed inhibition of SP secretion in this study represents a notable but non-exclusive biochemical signature of midgut cell apoptosis. Although these phenotypic manifestations may reflect the secondary downstream effects of GABA-mediated metabolic

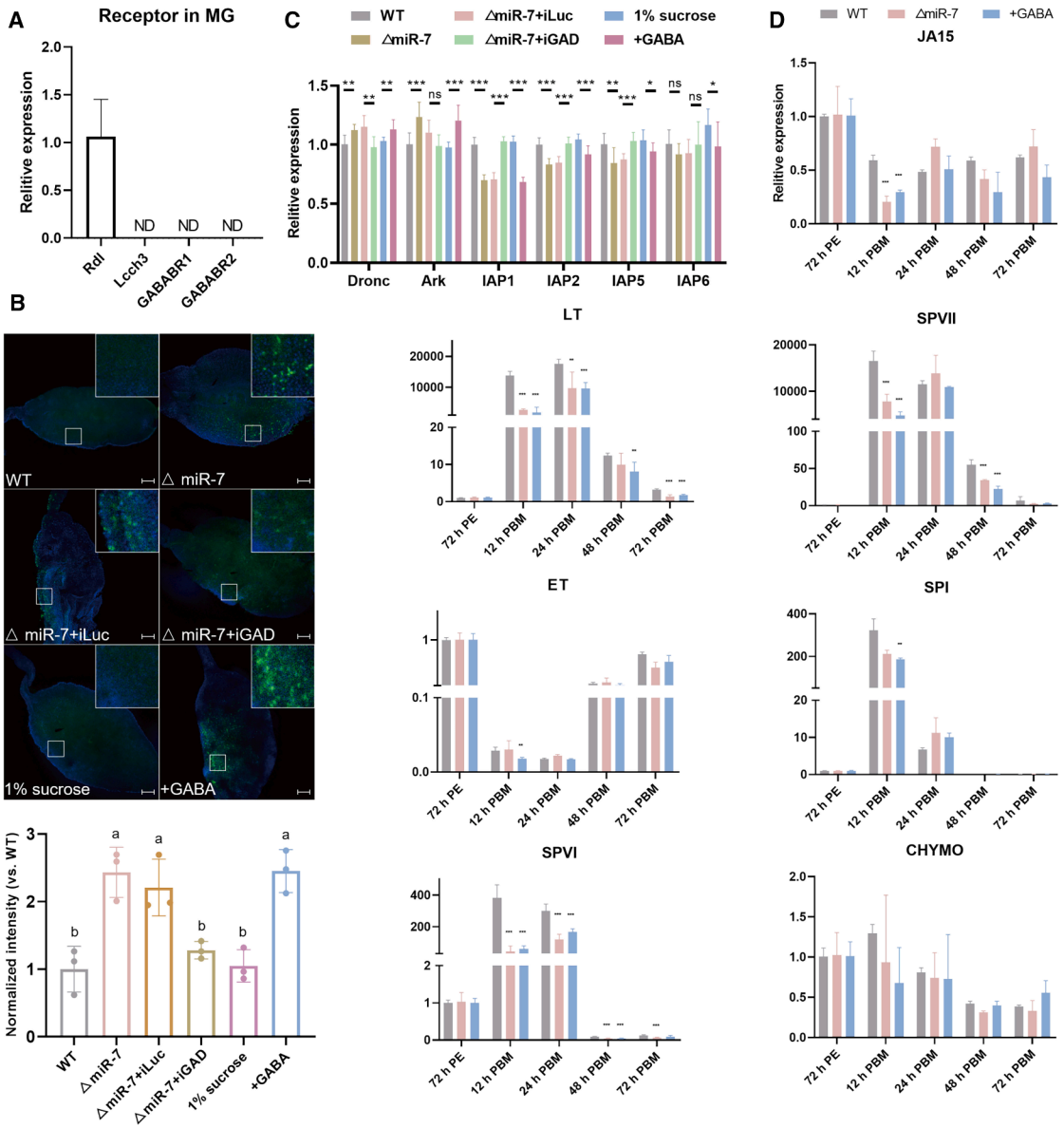

Figure 6. The reduction in serine protease activity represents a critical downstream consequence of the miR-7-GABA regulatory axis

(A) qPCR analysis reveals GABA receptor subtype expression profiles in midguts of WT females immediately PBM (0 h).

(B) Assessment of experimental intervention effects on midgut cell apoptosis was performed using TUNEL-based apoptosis detection (scale bar: 100 μm; blue fluorescence: DAPI; green fluorescence: TUNEL).

(C) Quantification of core apoptotic regulator expression profiles in midguts at 24 h PBM was conducted via qPCR.

(D) qPCR analysis demonstrates differential regulation in WT, *ΔmiR-7*, and GABA-fed females across multiple PBM time points.

Data are represented as means ± SEM. ns $p > 0.05$, *$p < 0.05$, **$p < 0.01$, and ***$p < 0.001$.

regulation, they provide critical insights into the complex interplay between neurotransmitter signaling and digestive function in *Ae. aegypti*. These findings hold significant translational implications. As a well-characterized neurotransmitter and drug target, the repellent activity of GABA against insects has been documented,[62–64] and the RDL receptor has been identified as a target of ivermectin and fluralaner in *Ae. aegypti.*[65] These observations highlight the potential of GABA-based therapeutics for vector control. Our work provides critical insights into the specific tissue targets of GABA signaling and establishes a translational framework for developing mosquito-specific repellents that target intestinal regulatory pathways. miR-7 not only regulates GABA synthesis but also modulates Glu metabolism in the midgut. As shown in Figures 3D and 4E, our data establish a significant correlation between hematophagic digestion dysfunction and reduced Glu consumption. Notably, despite Glu accumulation in the GABA-supplemented group (Figure 5F), midgut digestive defects remain unresolved. This experimental

evidence further corroborates the absence of a direct causal relationship between blood-meal digestion capacity and midgut Glu content. Collectively, this study delineates an innovative regulatory mechanism through the miR-7-GABA axis, in which digestive system homeostasis exerts systemic control over the reproductive processes in female *Ae*. *aegypti*.

Limitations of the study

Our findings establish the regulatory role of miR-7 in female reproductive fitness. However, for experiments with a large sample size (Figures 3G, 3H, 4I, 4J, S6F, and S7B), the random sampling methodology applied in genotyping analyses introduces variability. While this variability does not negate the overall trend of results, it must be factored into the interpretation of exact reproductive inhibition rates. Although the physiological changes observed 24 h PBM are sufficient to support our conclusions, whether miR-7 regulates the physiological state of *Ae*. *aegypti* at other PBM time points remains to be investigated. miR-7 serves as a central regulator within the hierarchical network governing lipid metabolism in *Ae*. *aegypti*. While orchestrating midgut digestive physiology through classical pathways, its capacity to modulate lipid metabolic processes via non-intestinal tissues remains to be fully defined. While GABA treatment in the digestive tract has demonstrated the tissue specificity of the regulatory network proposed in this study, the broader organismal effects of GABAergic modulation in this organ remain largely unknown. The activation of diverse apoptotic pathways by GABA has been documented across biological systems.[30,31] However, the molecular mechanism underlying its pro-apoptotic effect on midgut epithelial cells remains to be elucidated in this investigation. Our results confirm that midgut miR-7 in female *Ae*. *aegypti* directly targets GAD to regulate GABA synthesis, thereby reducing reproductive fitness by affecting midgut function. Despite the limitations of this study, these findings offer practical relevance for developing vector control strategies focused on midgut modulation to mitigate disease transmission.

RESOURCE AVAILABILITY

Lead contact

Further information and requests for resources and reagents should be directed to the lead contact, Lin Ling (linglin1000@163.com).

Materials availability

Materials used in this study are available upon request.

Data and code availability

- Datasets supporting the current study will be shared by the lead contact upon request.
- The FASTQ sequencing data have been deposited at the Sequence Read Archive (SRA) database and are publicly available as of the date of publication. Accession numbers are listed in the key resources table.
- Any additional information required to reanalyze the data reported in this article is available from the lead contact upon request.

ACKNOWLEDGMENTS

We thank Professor Junhai Han (Southeast University) for providing the S2 cells. This study was supported by the National Natural Science Foundation of China (grant number 32470502 to L.L.). The graphical abstract was created using BioRender.com.

AUTHOR CONTRIBUTIONS

L.L. and J.C. conceived and implemented the project and wrote the manuscript.

DECLARATION OF INTERESTS

The authors declare no competing interests.

STAR★METHODS

Detailed methods are provided in the online version of this paper and include the following:

- KEY RESOURCES TABLE
- EXPERIMENTAL MODEL AND STUDY PARTICIPANT DETAILS
  - Mosquito rearing
- METHOD DETAILS
  - sRNA-seq and data processing
  - Quantitative real-time PCR assays of genes and miRNAs
  - Localization of miRNA and its targets by RNA FISH
  - Measurement of Glu, GABA, and HGB levels
  - RNA interference
  - *In vitro* luciferase reporter gene assays
  - Lipid droplet staining
  - Embryonic injection and genotyping
  - TUNEL staining
- QUANTIFICATION AND STATISTICAL ANALYSIS
  - Statistical analysis

SUPPLEMENTAL INFORMATION

Supplemental information can be found online at https://doi.org/10.1016/j.celrep.2025.115776.

Received: January 16, 2025
Revised: April 18, 2025
Accepted: May 12, 2025

REFERENCES

1. Kraemer, M.U.G., Reiner, R.C., Jr., Brady, O.J., Messina, J.P., Gilbert, M., Pigott, D.M., Yi, D., Johnson, K., Earl, L., Marczak, L.B., et al. (2019). Past and future spread of the arbovirus vectors *Aedes aegypti* and *Aedes albopictus*. Nat. Microbiol. *4*, 854–863. https://doi.org/10.1038/s41564-019-0376-y.
2. Kraemer, M.U.G., Sinka, M.E., Duda, K.A., Mylne, A.Q.N., Shearer, F.M., Barker, C.M., Moore, C.G., Carvalho, R.G., Coelho, G.E., Van Bortel, W., et al. (2015). The global distribution of the arbovirus vectors *Aedes aegypti* and. Elife *4*, e08347. https://doi.org/10.7554/eLife.08347.
3. Brackney, D.E., LaReau, J.C., and Smith, R.C. (2021). Frequency matters: How successive feeding episodes by blood-feeding insect vectors influences disease transmission. PLoS Pathog. *17*, e1009590. https://doi.org/10.1371/journal.ppat.1009590.
4. Venkataraman, K., Shai, N., Lakhiani, P., Zylka, S., Zhao, J., Herre, M., Zeng, J., Neal, L.A., Molina, H., Zhao, L., and Vosshall, L.B. (2023). Two novel, tightly linked, and rapidly evolving genes underlie *Aedes aegypti* mosquito reproductive resilience during drought. Elife *12*, e80489. https://doi.org/10.7554/eLife.80489.
5. Gulia-Nuss, M., Elliot, A., Brown, M.R., and Strand, M.R. (2015). Multiple factors contribute to an autogenous reproduction by the mosquito *Aedes aegypti*. J. Insect Physiol. *82*, 8–16. https://doi.org/10.1016/j.jinsphys.2015.08.001.
6. Wang, X., Ding, Y., Lu, X., Geng, D., Li, S., Raikhel, A.S., and Zou, Z. (2021). The ecdysone-induced protein 93 is a key factor regulating gonadotrophic cycles in the adult female mosquito *Aedes aegypti*. Proc. Natl. Acad. Sci. USA *118*, e2021910118. https://doi.org/10.1073/pnas.2021910118.

7. Zhou, G., Pennington, J.E., and Wells, M.A. (2004). Utilization of pre-existing energy stores of female *Aedes aegypti* mosquitoes during the first gonotrophic cycle. Insect Biochem. Mol. Biol. *34*, 919–925. https://doi.org/10.1016/j.ibmb.2004.05.009.

8. Briegel, H., Knüsel, I., and Timmermann, S.E. (2001). *Aedes aegypti*: size, reserves, survival, and flight potential. J. Vector Ecol. *26*, 21–31.

9. Barredo, E., and DeGennaro, M. (2020). Not just from blood: mosquito nutrient acquisition from nectar sources. Trends Parasitol. *36*, 473–484. https://doi.org/10.1016/j.pt.2020.02.003.

10. Isoe, J., Rascón, A.A., Jr., Kunz, S., and Miesfeld, R.L. (2009). Molecular genetic analysis of midgut serine proteases in *Aedes aegypti* mosquitoes. Insect Biochem. Mol. Biol. *39*, 903–912. https://doi.org/10.1016/j.ibmb.2009.10.008.

11. Rascon, A.A.J., Gearin, J., Isoe, J., and Miesfeld, R.L. (2011). In vitro activation and enzyme kinetic analysis of recombinant midgut serine proteases from the Dengue vector mosquito *Aedes aegypti*. BMC Biochem. *12*, 43. https://doi.org/10.1186/1471-2091-12-43.

12. Bian, G., Raikhel, A.S., and Zhu, J. (2008). Characterization of a juvenile hormone-regulated chymotrypsin-like serine protease gene in *Aedes aegypti* mosquito. Insect Biochem. Mol. Biol. *38*, 190–200. https://doi.org/10.1016/j.ibmb.2007.10.008.

13. Zhang, X., Aksoy, E., Girke, T., Raikhel, A.S., and Karginov, F.V. (2017). Transcriptome-wide microRNA and target dynamics in the fat body during the gonadotrophic cycle of *Aedes aegypti*. Proc. Natl. Acad. Sci. USA *114*, E1895–E1903. https://doi.org/10.1073/pnas.1701474114.

14. Dou, X., Chen, K., Brown, M.R., and Strand, M.R. (2023). Multiple endocrine factors regulate nutrient mobilization and storage in *Aedes aegypti* during a gonadotrophic cycle. Insect Sci. *30*, 425–442. https://doi.org/10.1111/1744-7917.13110.

15. Ziegler, R., and Ibrahim, M.M. (2001). Formation of lipid reserves in fat body and eggs of the yellow fever mosquito, *Aedes aegypti*. J. Insect Physiol. *47*, 623–627. https://doi.org/10.1016/s0022-1910(00)00158-x.

16. Naeli, P., Winter, T., Hackett, A.P., Alboushi, L., and Jafarnejad, S.M. (2023). The intricate balance between microRNA-induced mRNA decay and translational repression. FEBS J. *290*, 2508–2524. https://doi.org/10.1111/febs.16422.

17. Rani, V., and Sengar, R.S. (2022). Biogenesis and mechanisms of microRNA-mediated gene regulation. Biotechnol. Bioeng. *119*, 685–692. https://doi.org/10.1002/bit.28029.

18. Catalanotto, C., Cogoni, C., and Zardo, G. (2016). MicroRNA in control of gene expression: an overview of nuclear functions. Int. J. Mol. Sci. *17*, 1712. https://doi.org/10.3390/ijms17101712.

19. Jonas, S., and Izaurralde, E. (2015). Towards a molecular understanding of microRNA-mediated gene silencing. Nat. Rev. Genet. *16*, 421–433. https://doi.org/10.1038/nrg3965.

20. Bryant, B., Macdonald, W., and Raikhel, A.S. (2010). microRNA miR-275 is indispensable for blood digestion and egg development in the mosquito *Aedes aegypti*. Proc. Natl. Acad. Sci. USA *107*, 22391–22398. https://doi.org/10.1073/pnas.1016230107.

21. Zhang, X., and Raikhel, A.S. (2021). Hormonal regulation of microRNA expression dynamics in the gut of the yellow fever mosquito *Aedes aegypti*. RNA Biol. *18*, 1682–1691. https://doi.org/10.1080/15476286.2020.1864181.

22. Liu, S., Lucas, K.J., Roy, S., Ha, J., and Raikhel, A.S. (2014). Mosquito-specific microRNA-1174 targets serine hydroxymethyltransferase to control key functions in the gut. Proc. Natl. Acad. Sci. USA *111*, 14460–14465. https://doi.org/10.1073/pnas.1416278111.

23. Zhao, B., Lucas, K.J., Saha, T.T., Ha, J., Ling, L., Kokoza, V.A., Roy, S., and Raikhel, A.S. (2017). MicroRNA-275 targets sarco/endoplasmic reticulum Ca^{2+} adenosine triphosphatase (SERCA) to control key functions in the mosquito gut. PLoS Genet. *13*, e1006943. https://doi.org/10.1371/journal.pgen.1006943.

24. Frontali, N. (1961). Activity of glutamic acid decarboxylase in insect nerve tissue. Nature *191*, 178–179. https://doi.org/10.1038/191178b0.

25. Ilg, T., Berger, M., Noack, S., Rohwer, A., and Gaßel, M. (2013). Glutamate decarboxylase of the parasitic arthropods Ctenocephalides felis and Rhipicephalus microplus: gene identification, cloning, expression, assay development, identification of inhibitors by high throughput screening and comparison with the orthologs from Drosophila melanogaster and mouse. Insect Biochem. Mol. Biol. *43*, 162–177. https://doi.org/10.1016/j.ibmb.2012.11.001.

26. Sanders, H.R., Evans, A.M., Ross, L.S., and Gill, S.S. (2003). Blood meal induces global changes in midgut gene expression in the disease vector, *Aedes aegypti*. Insect Biochem. Mol. Biol. *33*, 1105–1122. https://doi.org/10.1016/s0965-1748(03)00124-3.

27. Alabaster, A., Isoe, J., Zhou, G., Lee, A., Murphy, A., Day, W.A., and Miesfeld, R.L. (2011). Deficiencies in acetyl-CoA carboxylase and fatty acid synthase 1 differentially affect eggshell formation and blood meal digestion in *Aedes aegypti*. Insect Biochem. Mol. Biol. *41*, 946–955. https://doi.org/10.1016/j.ibmb.2011.09.004.

28. Briegel, H., Hefti, M., and DiMarco, E. (2002). Lipid metabolism during sequential gonotrophic cycles in large and small female *Aedes aegypti*. J. Insect Physiol. *48*, 547–554. https://doi.org/10.1016/s0022-1910(02)00072-0.

29. Lau, M.J., Nie, S., Yang, Q., Harshman, L.G., Mao, C., Williamson, N.A., and Hoffmann, A.A. (2023). Lipidomic profiling reveals concerted temporal patterns of functionally related lipids in *Aedes aegypti* females following blood feeding. Metabolites *13*, 421. https://doi.org/10.3390/metabo13030421.

30. An, J., Seok, H., and Ha, E.M. (2021). GABA-producing Lactobacillus plantarum inhibits metastatic properties and induces apoptosis of 5-FU-resistant colorectal cancer cells via $GABA_B$ receptor signaling. J. Microbiol. *59*, 202–216. https://doi.org/10.1007/s12275-021-0562-5.

31. Tian, H., Wu, J.X., Shan, F.X., Zhang, S.N., Cheng, Q., Zheng, J.N., and Pei, D.S. (2015). Gamma-aminobutyric acid induces tumor cells apoptosis via GABABR1·β-arrestins. JNKs signaling module. Cell Biochem. Biophys. *71*, 679–688. https://doi.org/10.1007/s12013-014-0247-3.

32. Liu, Q., and Clem, R.J. (2011). Defining the core apoptosis pathway in the mosquito disease vector Aedes aegypti: the roles of iap1, ark, dronc, and effector caspases. Apoptosis *16*, 105–113. https://doi.org/10.1007/s10495-010-0558-9.

33. Cui, Y., and Franz, A.W.E. (2020). Heterogeneity of midgut cells and their differential responses to blood meal ingestion by the mosquito, Aedes aegypti. Insect Biochem. Mol. Biol. *127*, 103496. https://doi.org/10.1016/j.ibmb.103496.

34. He, Y.Z., Ding, Y., Wang, X., Zou, Z., and Raikhel, A.S. (2021). E93 confers steroid hormone responsiveness of digestive enzymes to promote blood meal digestion in the midgut of the mosquito *Aedes aegypti*. Insect Biochem. Mol. Biol. *134*, 103580. https://doi.org/10.1016/j.ibmb.2021.103580.

35. Fernandes, K.M., Tomé, H.V.V., Miranda, F.R., Gonçalves, W.G., Pascini, T.V., Serrão, J.E., and Martins, G.F. (2019). *Aedes aegypti* larvae treated with spinosad produce adults with damaged midgut and reduced fecundity. Chemosphere *221*, 464–470. https://doi.org/10.1016/j.chemosphere.2019.01.068.

36. Bombaca, A.C.S., Gandara, A.C.P., Ennes-Vidal, V., Bottino-Rojas, V., Dias, F.A., Farnesi, L.C., Sorgine, M.H., Bahia, A.C., Bruno, R.V., and Menna-Barreto, R.F.S. (2021). *Aedes aegypti* infection with trypanosomatid *Strigomonas culicis* alters midgut redox metabolism and reduces mosquito reproductive fitness. Front. Cell. Infect. Microbiol. *11*, 732925. https://doi.org/10.3389/fcimb.2021.732925.

37. Hagedorn, H.H., and Fallon, A.M. (1973). Ovarian control of vitellogenin synthesis by the fat body in *Aedes aegypti*. Nature *244*, 103–105. https://doi.org/10.1038/244103a0.

38. Gaio, A.D.O., Gusmão, D.S., Santos, A.V., Berbert-Molina, M.A., Pimenta, P.F.P., and Lemos, F.J.A. (2011). Contribution of midgut bacteria to blood digestion and egg production in *aedes aegypti* (diptera: culicidae) (L.). Parasit. Vectors *4*, 105. https://doi.org/10.1186/1756-3305-4-105.

39. Hawkey, C.M., Bennett, P.M., Gascoyne, S.C., Hart, M.G., and Kirkwood, J.K. (1991). Erythrocyte size, number and haemoglobin content in

vertebrates. Br. J. Haematol. *77*, 392–397. https://doi.org/10.1111/j.1365-2141.1991.tb08590.x.

40. Pascoa, V., Oliveira, P.L., Dansa-Petretski, M., Silva, J.R., Alvarenga, P.H., Jacobs-Lorena, M., and Lemos, F.J.A. (2002). *Aedes aegypti* peritrophic matrix and its interaction with heme during blood digestion. Insect Biochem. Mol. Biol. *32*, 517–523. https://doi.org/10.1016/s0965-1748(01)00130-8.
41. Eggleston, H., and Adelman, Z.N. (2020). Transcriptomic analyses of *Aedes aegypti* cultured cells and ex vivo midguts in response to an excess or deficiency of heme: a quest for transcriptionally-regulated heme transporters. BMC Genom. *21*, 604. https://doi.org/10.1186/s12864-020-06981-5.
42. Downe, A.E. (1975). Internal regulation of rate of digestion of blood meals in the mosquito, *Aedes aegypti*. J. Insect Physiol. *21*, 1835–1839. https://doi.org/10.1016/0022-1910(75)90250-4.
43. O'Donoghue, A.J., Liu, C., Simington, C.J., Montermoso, S., Moreno-Galvez, E., Serafim, M.S.M., Burata, O.E., Lucero, R.M., Nguyen, J.T., Fong, D., et al. (2025). Comprehensive proteolytic profiling of *Aedes aegypti* mosquito midgut extracts: Unraveling the blood meal protein digestion system. PLoS Negl. Trop. Dis. *19*, e0012555. https://doi.org/10.1371/journal.pntd.0012555.
44. Gooding, R.H. (1966). Physiological aspects of digestion of the blood meal by *Aedes aegypti* (Linnaeus) and *Culex* fatigans Wiedemann. J. Med. Entomol. *3*, 53–60. https://doi.org/10.1093/jmedent/3.1.53.
45. Noriega, F.G., Pennington, J.E., Barillas-Mury, C., Wang, X.Y., and Wells, M.A. (1996). *Aedes aegypti* midgut early trypsin is post-transcriptionally regulated by blood feeding. Insect Mol. Biol. *5*, 25–29. https://doi.org/10.1111/j.1365-2583.1996.tb00037.x.
46. Thayer, D.W., Terzian, L.A., and Price, P.A. (1971). Digestion of the human blood-meal by the mosquito, *Aedes aegypti*. J. Insect Physiol. *17*, 2469–2473. https://doi.org/10.1016/0022-1910(71)90094-1.
47. Hixson, B., Bing, X.L., Yang, X., Bonfini, A., Nagy, P., and Buchon, N. (2022). A transcriptomic atlas of *Aedes aegypti* reveals detailed functional organization of major body parts and gut regional specializations in sugar-fed and blood-fed adult females. Elife *11*, e76132. https://doi.org/10.7554/eLife.76132.
48. Diag, A., Schilling, M., Klironomos, F., Ayoub, S., and Rajewsky, N. (2018). Spatiotemporal m(i)RNA architecture and 3' UTR regulation in the *C. elegans* germline. Dev. Cell *47*, 785–800.e8. https://doi.org/10.1016/j.devcel.2018.10.005.
49. Sambandan, S., Akbalik, G., Kochen, L., Rinne, J., Kahlstatt, J., Glock, C., Tushev, G., Alvarez-Castelao, B., Heckel, A., and Schuman, E.M. (2017). Activity-dependent spatially localized miRNA maturation in neuronal dendrites. Science *355*, 634–637. https://doi.org/10.1126/science.aaf8995.
50. DeVeale, B., Swindlehurst-Chan, J., and Blelloch, R. (2021). The roles of microRNAs in mouse development. Nat. Rev. Genet. *22*, 307–323. https://doi.org/10.1038/s41576-020-00309-5.
51. Brosnan, C.A., Palmer, A.J., and Zuryn, S. (2021). Cell-type-specific profiling of loaded miRNAs from *Caenorhabditis elegans* reveals spatial and temporal flexibility in Argonaute loading. Nat. Commun. *12*, 2194. https://doi.org/10.1038/s41467-021-22503-7.
52. Aboobaker, A.A., Tomancak, P., Patel, N., Rubin, G.M., and Lai, E.C. (2005). Drosophila microRNAs exhibit diverse spatial expression patterns during embryonic development. Proc. Natl. Acad. Sci. USA *102*, 18017–18022. https://doi.org/10.1073/pnas.0508823102.
53. Liufu, Z., Zhao, Y., Guo, L., Miao, G., Xiao, J., Lyu, Y., Chen, Y., Shi, S., Tang, T., and Wu, C.I. (2017). Redundant and incoherent regulations of multiple phenotypes suggest microRNAs' role in stability control. Genome Res. *27*, 1665–1673. https://doi.org/10.1101/gr.222505.117.
54. Hausser, J., and Zavolan, M. (2014). Identification and consequences of miRNA-target interactions–beyond repression of gene expression. Nat. Rev. Genet. *15*, 599–612. https://doi.org/10.1038/nrg3765.
55. Ling, L., Kokoza, V.A., Zhang, C., Aksoy, E., and Raikhel, A.S. (2017). MicroRNA-277 targets *insulin-like peptides 7* and *8* to control lipid metabolism and reproduction in *Aedes aegypti* mosquitoes. Proc. Natl. Acad. Sci. USA *114*, E8017–E8024. https://doi.org/10.1073/pnas.1710970114.
56. Modi, J.P., Prentice, H., and Wu, J.Y. (2015). Regulation of GABA neurotransmission by glutamic acid decarboxylase (GAD). Curr. Pharm. Des. *21*, 4939–4942. https://doi.org/10.2174/1381612821666150917094343.
57. Kim, K., and Yoon, H. (2023). Gamma-aminobutyric acid signaling in damage response, metabolism, and disease. Int. J. Mol. Sci. *24*, 4584. https://doi.org/10.3390/ijms24054584.
58. Andersen, J.V., Schousboe, A., and Wellendorph, P. (2023). Astrocytes regulate inhibitory neurotransmission through GABA uptake, metabolism, and recycling. Essays Biochem. *67*, 77–91. https://doi.org/10.1042/EBC20220208.
59. Auteri, M., Zizzo, M.G., Mastropaolo, M., and Serio, R. (2014). Opposite role played by GABAA and GABAB receptors in the modulation of peristaltic activity in mouse distal colon. Eur. J. Pharmacol. *731*, 93–99. https://doi.org/10.1016/j.ejphar.2014.03.003.
60. Fargeas, M.J., Fioramonti, J., and Bueno, L. (1988). Central and peripheral action of GABAA and GABAB agonists on small intestine motility in rats. Eur. J. Pharmacol. *150*, 163–169. https://doi.org/10.1016/0014-2999(88)90763-7.
61. Jin, H., Han, H., Song, G., Oh, H.J., and Lee, B.Y. (2024). Anti-obesity effects of GABA in C57BL/6J mice with high-fat diet-induced obesity and 3T3-L1 adipocytes. Int. J. Mol. Sci. *25*, 995. https://doi.org/10.3390/ijms25020995.
62. Buckingham, S.D., Ihara, M., Sattelle, D.B., and Matsuda, K. (2017). Mechanisms of action, resistance and toxicity of insecticides targeting GABA receptors. Curr. Med. Chem. *24*, 2935–2945. https://doi.org/10.2174/0929867324666170613075736.
63. Bown, A.W., Macgregor, K.B., and Shelp, B.J. (2006). Gamma-aminobutyrate: defense against invertebrate pests? Trends Plant Sci. *11*, 424–427. https://doi.org/10.1016/j.tplants.2006.07.002.
64. Nakao, T., and Banba, S. (2021). Mechanisms underlying the selectivity of meta-diamides between insect resistance to dieldrin (RDL) and human gamma-aminobutyric acid (GABA) and glycine receptors. Pest Manag. Sci. *77*, 3744–3752. https://doi.org/10.1002/ps.6116.
65. Wang, Q., Wang, H., Zhang, Y., Chen, J., Upadhyay, A., Bhowmick, B., Hang, J., Wu, S., Liao, C., and Han, Q. (2022). Functional analysis reveals ionotropic GABA receptor subunit RDL is a target site of ivermectin and fluralaner in the yellow fever mosquito, *Aedes aegypti*. Pest Manag. Sci. *78*, 4173–4182. https://doi.org/10.1002/ps.7035.
66. Guo, Z., Zhu, L., Cheng, Z., Dong, L., Guo, L., Bai, Y., Wu, Q., Wang, S., Yang, X., Xie, W., et al. (2024). A midgut transcriptional regulatory loop favors an insect host to withstand a bacterial pathogen. Innovation *5*, 100675. https://doi.org/10.1016/j.xinn.2024.100675.
67. Ling, L., and Raikhel, A.S. (2023). Amino acid-dependent regulation of insulin-like peptide signaling is mediated by TOR and GATA factors in the disease vector mosquito *Aedes aegypti*. Proc. Natl. Acad. Sci. USA *120*, e2303234120. https://doi.org/10.1073/pnas.2303234120.
68. Yang, M., Wang, Y., Jiang, F., Song, T., Wang, H., Liu, Q., Zhang, J., Zhang, J., and Kang, L. (2016). miR-71 and miR-263 jointly regulate target genes chitin synthase and chitinase to control locust molting. PLoS Genet. *12*, e1006257. https://doi.org/10.1371/journal.pgen.1006257.
69. Kokoza, V., Ahmed, A., Woon Shin, S., Okafor, N., Zou, Z., and Raikhel, A.S. (2010). Blocking of Plasmodium transmission by cooperative action of Cecropin A and Defensin A in transgenic *Aedes aegypti* mosquitoes. Proc. Natl. Acad. Sci. USA *107*, 8111–8116. https://doi.org/10.1073/pnas.1003056107.

STAR★METHODS

KEY RESOURCES TABLE

REAGENT or RESOURCE	SOURCE	IDENTIFIER
Biological samples		
Aedes aegypti	Lab stock	N/A
White-feathered broilers	Lab stock	N/A
S2 cells	Lab stock	N/A
Chemicals, peptides, and recombinant proteins		
Cas9 protein	PNA Bio	CP01
GABA	Macklin	A794384
miRNA mimics	Qiagen	219600
psiCHECK-2 Vector	Promega	C8021
T4 DNA Ligase	NEB	M0202V
Nile red	Sango	A606340
Trizol	Vazyme	R411
PBS	Sango	E607008
Critical commercial assays		
MEGAscript™ T7 Transcription Kit	Invitrogen	AM1334
MEGAclear™ Transcription Clean-Up Kit	Invitrogen	AM1908
FastPure Tissue/Bacteria DNA Isolation Mini Kit	Vazyme	DC112
Taq Pro Universal SYBR qPCR Master Mix	Vazyme	Q712
HiScript III RT SuperMix for qPCR (+gDNA wiper)	Vazyme	R323
miRNA First-Strand cDNA Synthesis SuperMix	Transgen	AT351
Lipofectamine 3000	Invitrogen	L3000015
Hemoglobin Microplate Assay Kit	Absin	abs580111
Insect Glutamic acid Microplate Assay Kit	Meimian	N/A
Insect Gamma-aminobutyric acid Microplate Assay Kit	Meimian	N/A
APO™ One-Step TUNEL Apoptosis Kit	Ribo	C11012
Dual-Luciferase® Reporter Assay System	Promega	E1910
Software and algorithms		
Prism 8	GraphPad	https://www.graphpad.com
ZEN 3.1	Carl Zeiss	https://www.zeiss.com/microscopy/en/products/software/zeiss-zen.html
Deposited data		
sRNA-seq data	this paper	SRA: PRJNA1209617

EXPERIMENTAL MODEL AND STUDY PARTICIPANT DETAILS

Mosquito rearing

The eggs were laid on a humidified filter paper. Larvae were reared in water maintained at 27°C and supplemented with commercial fish food pellets (Yee). Adult mosquitoes were housed in cages maintained at 27°C and 80% relative humidity and provided with 10% sucrose solution and sterile water as dietary resources. Blood feeding assays on adult mosquitoes were conducted on white-feathered broilers. All vertebrate animal handling protocols were approved by the Experimental Ethics Committee of Southeast University.

METHOD DETAILS

sRNA-seq and data processing

Each sample comprised 30 female *Ae*. *aegypti* midguts with three independent biological replicates per experimental group. Total RNA was extracted from female midguts 72 h PE and 24 h PBM using TRIzol (Vazyme) and treated with DNase I (NEB). The RNA

purity was assessed by measuring the A260/A280 ratio using a NanoDrop OneC Spectrophotometer (Thermo Fisher Scientific). RNA integrity was validated using a LabChip GX Touch Nucleic Acid Analyzer (Revvity). Qualified small RNA concentrations were quantified with a Qubit 3.0 Fluorometer and the Qubit miRNA Assay Kit (Thermo Fisher Scientific). The miRNA library was constructed using the QIAseq miRNA Library Kit (Qiagen) following the manufacturer's instructions. The amplified libraries were purified and size-selected (180 bp) by magnetic bead-based separation. Libraries were sequenced on the NovaSeq X Plus platform (Illumina) using paired-end 150 bp (PE150) sequencing. Raw sequencing data were subjected to quality control (QC) to ensure suitability for downstream analysis. After deduplication, sRNAs (18–30 nt) were retained for analysis. The reads were mapped against the *Aedes aegypti* reference genome (release-60) using the Bowtie software to identify known and novel miRNAs. Expression levels were normalized to transcripts per million. Differentially expressed miRNAs were identified using EdgeR with the criteria of $|\log_{10}\text{-fold change}| \geq 1$ and false discovery rate <0.05. Cluster analysis was performed based on these criteria. Gene Ontology terms and KEGG pathway enrichment analyses (http://www.genome.jp/kegg/) of the target genes were performed using the *Profiler R* package.

Quantitative real-time PCR assays of genes and miRNAs

The composition of samples and the extraction of total RNA were described in the "sRNA - seq and data processing" section. A constant amount of total RNA (500 ng) was reverse-transcribed into cDNA using either the HiScript III RT SuperMix for qPCR (+gDNA Wiper) kit or the miRNA First-Strand cDNA Synthesis SuperMix kit. Following 10-fold dilution, cDNA samples were amplified using Taq Pro Universal SYBR qPCR Master Mix (Vazyme). And signal collection was performed on CFX96 qPCR system (Bio-Rad) according to the manufacturer's instructions. U6 or RPS7 was selected as the internal reference gene, and relative expression analysis was conducted using the $2^{-\Delta\Delta Ct}$ method. Primer sequences for qPCR analysis are detailed in SI Appendix, Table S3. All the qPCR experiments were conducted with $\geq$3 biological replicates. The reagent specifications are listed in the key resources table.

Localization of miRNA and its targets by RNA FISH

A two-color fluorescence *in situ* hybridization analysis was performed to visualize miR-7 and its target gene GAD in mosquito guts, following the protocol described by Guo et al.[66] Briefly, intestinal tissue samples underwent sequential processing steps including: fixation, dehydration, sectioning, pre-hybridization treatment, hybridization, washing, counterstaining, and mounting. Samples were stored under dark conditions following completion of all procedures. Confocal microscopy was performed using the Zeiss LSM 900 system (Carl Zeiss Microscopy GmbH). Excitation were carried out at 555 nm (Cy3) and 492nm (FAM), and images were captured using ZEN 3.1 software (Zeiss). The specific antisense RNA probes labeled with Cy3 (5′-Cy3- ACAACAAAAUCACUAGUC UUCCA-3′) for miR-7 detection and with FAM (5′-FAM-UGAAGUGAAUAGUUGAGCA-3′) for GAD detection were commercially synthesized (Sangon Biotech). The scrambled probe with Cy3 (5′-Cy3-UUGUACUACACAAAAGUACUG-3′) for miRNA and with FAM (5′-FAM-UUGUACUACACAAAAGUACUG-3′) for mRNA were used as negative controls.

Measurement of Glu, GABA, and HGB levels

Gut lysates in phosphate-buffered saline (PBS) were collected from female mosquitoes. The concentrations of Glu and GABA were quantified using ELISA kits (Jiangsu Meimian Industrial Co., Ltd.), whereas HGB levels were measured using an HGB assay kit (Absin). All assays were performed according to manufacturer's instructions. Optical density values were determined at 450 nm for Glu/GABA detection and 435 nm for HGB quantification using a Varioskan Flash Multimode Reader (Thermo Fisher Scientific).

RNA interference

The methodology for RNA interference was described in detail elsewhere.[67] Female mosquitoes were anesthetized using a cold plate and microinjected with 1 μg/300 nL dsRNA targeting specific genes into the thoracic region. The injected mosquitoes were recovered under standard rearing conditions (27°C, 80% humidity) for 36 h. Gene silencing efficiency was quantified by qPCR analysis. Primer sequences for the target genes are listed in the SI Appendix (Table S3).

In vitro luciferase reporter gene assays

An approximately 120-bp fragment encompassing the predicted miR-7 target sites in the *GAD* gene was cloned into the *psiCHECK-2* dual-luciferase reporter vector (Promega). Mutations were introduced to disrupt miRNA-binding specificity by altering 20 nt of the target sites, including the region complementary to the miR-7 seed sequence. Co-transfection assays in S2 cells were performed using the methodology described by Yang et al.[68] Transfected cells were processed per the Dual-Luciferase Reporter Assay System kit guidelines. Signal intensities were quantified at 480 nm (Renilla luciferase) and 560 nm (Firefly luciferase) using the Varioskan Flash Multimode Reader (Thermo Fisher Scientific). Detailed reagent information is provided in the key resources table.

Lipid droplet staining

Fat body tissues were incubated in Nile red staining solution (20% glycerol in PBS containing a 1:10,000 dilution of 10% Nile red stock solution in dimethyl sulfoxide [DMSO]) for 15 min at room temperature. Confocal microscopy was performed using the Zeiss LSM 900 system (Carl Zeiss Microscopy GmbH). Excitation was carried out at 543 nm, and images were captured using ZEN 3.1 software (Zeiss). Detailed reagent information is provided in the key resources table.

Embryonic injection and genotyping

The synthesis of sgRNA has been described in detail in our previous study.[55] Primer sequences for sgRNA target design are listed in the SI Appendix, Table S3. Briefly, a mixture of sgRNAs (40 ng/μL) and Cas9 protein (333 ng/μL) was microinjected into pre-gastrulation embryos. They hatched 5 d after injection and were reared to adulthood according to the described protocol.[69] Females were crossed and blood-fed for phenotypic analysis. Genotyping was conducted by examining the exuviae shed during the pupal stage of the first transgenic generation. For experimental groups with fewer than nine biological replicates, complete genotyping was performed for all female mosquitoes. In contrast, groups containing 10 or more replicates (Figures 3G, 3H, 4I, 4J, S6F, and S7B) employed a randomized sampling strategy (20% sampling rate) to ensure statistical efficiency while maintaining experimental accuracy. Reagent details are provided in the key resources table.

TUNEL staining

Apoptotic cell death rates were quantified through terminal deoxynucleotidyl transferase-mediated dUTP nick end labeling (TUNEL) assays. Midgut tissues were processed following manufacturer protocols for the APO One-Step TUNEL Apoptosis Kit (Ribo). Confocal microscopy was performed using the Zeiss LSM 900 system (Carl Zeiss Microscopy GmbH). Excitation were carried out at 492 nm, and images were captured using ZEN 3.1 software (Zeiss).

QUANTIFICATION AND STATISTICAL ANALYSIS

Statistical analysis

All data are presented as the mean ± standard error of the mean (SEM). Comparisons between groups were performed using the Student's t test, with significance levels defined as follows: $^{*}p < 0.05$, $^{**}p < 0.01$, and $^{***}p < 0.001$. Statistical analyses were performed using GraphPad Prism version 8.